OPTICAL PROPERTIES OF CARBON DOTS

DEGREE IN CHEMISTRY

Marc Ávila Forés

Universidad Jaume I

Academic course 2016-2017

ABBREVIATIONS

GQDs: *Graphene quantum dots*

CDs: *Carbon dots*

QDs: *Quantum dots*

DFT: *Density Functional Theory*

DFTB: *Density-Functional Tight-Binding*

PEG: *Polyethylene glycol*

nR: *size of sheet graphene, n is the number of graphene that the molecule has as a radius.*

INDEX

1. INTRODUCTION

1. INTRODUCTION

1.1. Graphene

It was in 2006 when the carbon dots (CDs)[1] were discovered as a family of quantum dots (QDs). Since this moment CDs have attracted widespread attention and emerged as excellent fluorescent material. Especially, graphene dots are a class of zero-dimensional nanocarbons (carbon nanoparticles), which are less than 10 nm.

Graphene is a lattice of sp^2-carbon atoms with a hexagonal structure. This material has generated enormous excitement due to its unusual properties such as large surface area, superior mechanical flexibility and excellent thermal and chemical stability.

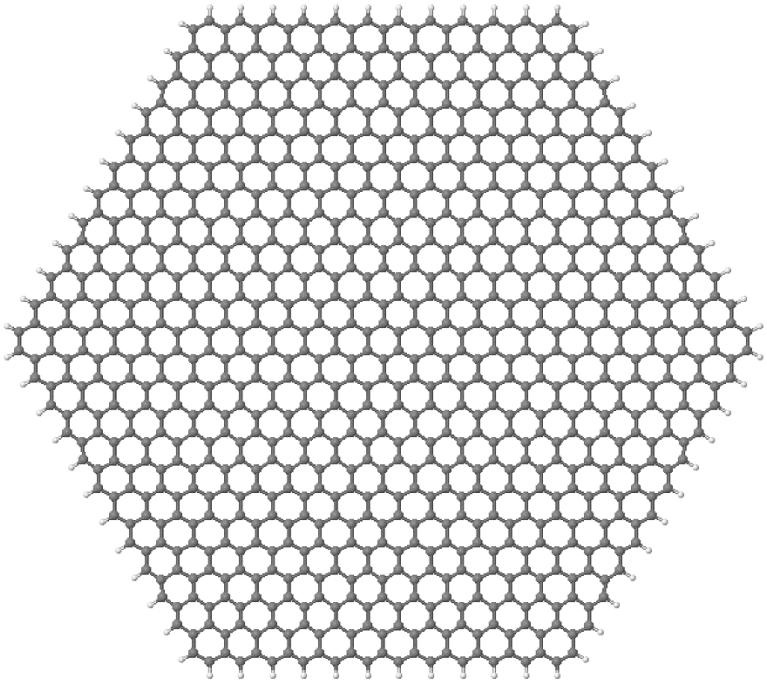

Figure 1: Structure of graphene

Graphene quantum dots (GQDs) are prepared in solution and they can incorporate a large number of functional groups on their surfaces, such as hydroxyl, epoxy, carboxyl…, which give rise to their high hydrophilicity and readiness for functionalization with various organic, polymeric or biological species. This GQDs display optical properties such as highly tunable photoluminescence from deep ultraviolet to near-infrared. To understand

[1] *Mandal, B., Sarkar, S. and Sarkar, P. (2012). Exploring the electronic structure of graphene quantum dots. Journal of Nanoparticle Research, 14(12).*

better this world, it is necessary to know the basic chemical and electronic structures of GQDs. Graphene quantum dots can be nanocrystals or amorphous nanoparticles linked by sp^2 bonding. After preparation of solutions, CDs are functionalized with complex surface groups, specially those containing oxygen, such as carboxyl or hydroxyl groups.

This surface functionalization sometimes modifies the physical properties of GQDs with the most obvious example being their solubility in aqueous and non-aqueous solvents as well as the large sp^2 π-conjugated structure endows GQDs with excellent characteristics, such as good photostability, high surface area and robust surface grafting through either π-π stacking or their surface functional groups.

The electronic structures of GQDs have been investigated and the results reveal that due to quantum confinement effect, the highest occupied molecular orbital (HOMO) and the lowest unoccupied molecular orbital (LUMO) of GQDs shift to higher and lower energy increasing dot size and reducing their HOMO-LUMO gap (ΔE_{L-H}). Meanwhile, other functional groups modulate the HOMO and LUMO levels, leaving unaltered the HOMO-LUMO gap. To study this levels is necessary the use of quantum mechanics methods.

1.2. Polyethylene glycol (PEG)

Polyethylene glycol is a well-known polymer. PEG may have different sizes, however the most commonly used for this kind of investigations is PEG-200, of which structure is $C_8H_{18}O_5$[2] (*Figure 2)*. The number represents the molecular mass; in this case the PEG-200 have a molecular mass of 200 Da (200 g/mol). This polymer is miscible in water. Furthermore, its level of toxicity is very low, and for this reason it is usually used for the investigation of new indicators of cancer[3].

It is an interesting molecule to link with graphene sheets, since it allows to change the photovoltaic properties of graphene due to the modification of the band gap ($\Delta E_{L\text{-}H}$). In addition, it is an easy reaction to do in the laboratory.

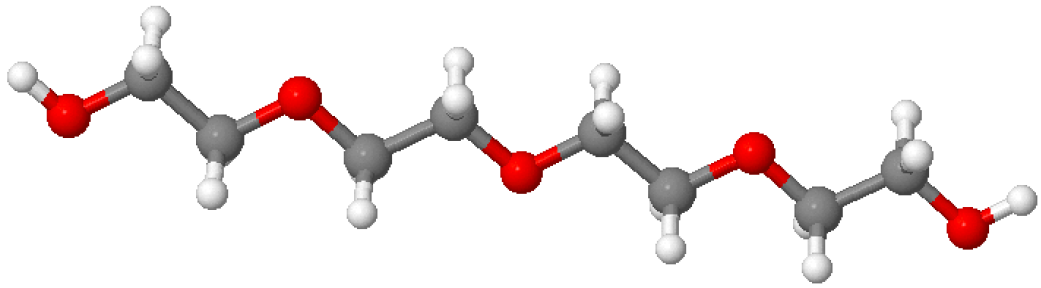

Figure 2: Structure of PEG-200.

[2] *Es.wikipedia.org. (2017). Polietilenglicol. Available at: https://es.wikipedia.org/wiki/Polietilenglicol.*
[3] *Yuan, F., Li, S., Fan, Z., Meng, X., Fan, L. and Yang, S. (2016). Shining carbon dots: Synthesis and biomedical and optoelectronic applications. Nano Today, 11(5), pp.565-586.*

1.3. Density Functional Method (DFT)

The problem of dealing with a system of N interacting electrons in an external potential, $Vext$, is traditionally expressed by the 3N-dimensional Schrödinger equation for the wave-function. With Density Functional Method[4] the problem can be dealt in terms of the electronic density distribution, $\rho(\vec{r})$. Therefore, use DFT means that the system only depends on the three spatial coordinates (x, y, z) and the spin (σ).

1.3.1. Hohenberg-Khon Theorems

DFT theory was developed by P. Hohenber and W. Khon. Their first theorem states that the density of nondegenerate fundamental state determines the external potential (and vice versa) and also allows to obtain properties of the system.

On the other hand, the second Hohenber-Khon[5] theorem, dubbed as Variational Theorem, shows that *the functional that delivers the ground-state energy of the system, delivers the lowest energy if and only if the input density is the true ground state density,* ρ_o.

1.3.2. The Kohn-Sham (KS) method

The expression for the energy in a system-dependent of the density function (electronic in the case of molecules under Born-Oppenhaimer approximation), *eq. 1*, can be written as:

$$E[\rho(\vec{r})] = T_{ni}[\rho(\vec{r})] + V_{ne}[\rho(\vec{r})] + V_{ee}[\rho(\vec{r})] + \Delta T[\rho(\vec{r})] + \Delta V_{ee}[\rho(\vec{r})] \qquad (1)$$

Where the first term[6] $\mathrm{T_{ni}}[\rho(\vec{r})]$, corresponds to the kinetic energy of the non-interacting electrons: The second term, $\mathrm{V_{ne}}[\rho(\vec{r})]$, corresponds to the nuclear-electron interaction; The third term, $\mathrm{V_{ee}}[\rho(\vec{r})]$, refers to the classical electron-electron repulsion; the fourth term,

---

[4] *Seifert, G. and Joswig, J. (2012). Density-functional tight binding-an approximate density-functional theory method. Wiley Interdisciplinary Reviews: Computational Molecular Science, 2(3), pp.456-465.*

[5] *Ayers, P., Golden, S. and Levy, M. (2006). Generalizations of the Hohenberg-Kohn theorem: I. Legendre Transform Constructions of Variational Principles for Density Matrices and Electron Distribution Functions. The Journal of Chemical Physics, 124(5), p.054101.*

[6] *Kaupp, M. (2001). Book Review: A Chemist's Guide to Density Functional Theory. By Wolfram Koch and Max C. Holthausen. Angewandte Chemie International Edition, 40(5), pp.963-964.*

$\Delta T[\rho(\vec{r})]$, is the correction to the kinetic energy emerging from the interaction of the electrons. The last term, $\Delta V_{ee}[\rho(\vec{r})]$, means the non-classical correction to the electron-electron repulsion energy. *Eq. 1* can be rewritten taking into account interaction between nuclei:

$$E = T_{ni}[\rho(r)] + V_{ne}[\rho(r)] + V_{ee}[\rho(r)] + V_{XC}[\rho(r)] + V_{nn}(R) \quad (2)$$

where N is the number of electrons, and the density for Slater-determinant wave function is given by *eq.3*:

$$\rho = \sum_{i=1}^{N} \langle \chi_i | \chi_i \rangle \quad (3)$$

It is important to note that the two last terms of (1), $(\ldots + \Delta T[\rho(\vec{r})] + \Delta V_{ee}[\rho(\vec{r})])$, have been included into a single one, V_{xc}. This new term is known as exchange-correlation[7] potential, which is the functional that contains all things that are unknown. Within the range of exchange correlation potentials, it is possible to classify them into three major types according to the approximations used in their estimation.

Local Density Approximation (LDA)

This model is based on the idea of a hypothetical uniform electron gas and, as a consequence, it is the only system for which the exact form of the correlation and the exchange functionals are known exactly. The E_{XC} can be written in the following form:

$$E_{XC}^{LDA}[\rho] = \int \rho \, V_{XC}\,[\rho] d\vec{r} \quad (4)$$

where the exchange-correlation energy is represented by $E_{XC}\,(\rho)$. On the other hand, the term V_{XC} could be separated in two terms, the exchange and correlation contributions:

$$V_{XC}\,[\rho] = V_X\,[\rho] + V_c\,[\rho] \quad (5)$$

[7] *M. A.L. Marques. (2010). Book review: A Primer in Density Functional Theory by C. Fiolhais, F. Nogueira and M. Marques. Springer.*

Generalized gradient approximation (GGA)

In GGA functionals, the information about density not only comes from a particular point $\vec{r}$, but also incorporates an additional term with information related to the gradient of the density, $\nabla\rho\ (\vec{r})$, thus allowing a non-homogeneous description of the real electron density. The expression for GGA can be written in the following form:

$$E_{XC}^{GGA}[\rho] = \int \rho\, V_{XC}\, \nabla\rho[\rho] d\vec{r} \qquad (6)$$

Like in LDA, the exchange-correlation term V_{XC}^{GGA} can be separated in correlation and exchange contributions.

The most usual GGA correlation functionals are:

i) The correlation functional of Lee, Yang and Parr, which includes both local and non-local terms) (LYP[8])

ii) Gradient-corrected correlation functional of Perdew, Burke and Ernzerhof (PBE[9]).

In the case of the exchange functional, the most common is the Becke's functional (B[10]), which includes the Slater corrections involving the gradient of the density. The combination of both, exchange and correlation, give place to the well-known functionals: BLYP and BPBE.

Nowadays exist a new brand of DFT functionals which are based on the generalized gradient approximation (GGA). This new generation are known as meta-GGA, and they introduce higher-order density gradient terms in order to improve the accuracy.

[8] *C. Lee, W. Yang, R. G. Parr, "Development of the Colle-Salvetti correlation-energy formula into a functional of the electron density", Phys. Rev. B, 1988, 37, 785-789.*

[9] *J. P. Perdew, M. Ernzerhof, and K. Burke, "Rationale for mixing exact exchange with density functional approximations", J. Chem. Phys., 1996 105, 9982.*

[10] *A. D. Becke. "Density-functional exchange-energy approximation with correct asymptotic behaviour", Phys. Rev. A 1988, 38, 3098-3100.*

Hybrid Functionals

As its names implies, hybrid functional methods consist in combine the exchange-correlation of GGA or meta-GGA with Hartree-Fock exchange. In these methods, the exchange amount of HF is determined empirically. The most famous hybrid functional method is B3LYP, composed by: Becke (B), three-parameter (3) and Lee-Yang-Parr (LYP). The expression for the exchange-correlation energy for B3LYP is:

$$E_{XC}^{B3LYP} = E_X^S + a_0(E_X^{HF} - E_X^S) + a_X(E_X^B - E_X^S) + a_C(E_C^{LYP} - E_C^{VWM}) + E_C^{VWM} \qquad (7)$$

Where $a_0, a_c \; and \; a_x$ are known. E_X^B is the exchange GGA Becke functional (B), E_C^{LYP} is the correlation GGA functional (LYP), E_C^{VWM} is an additional correlation LDA functional from Vocko, Wilk and Nusair (VWM[11]) and finally E_X^S is the Slater exchange functional[12].

[11] *S. H. Vosko, L. Wilk, and M. Nusair, "Accurate spin-dependent electron liquid correlation energies for local spin density calculations: A critical analysis," Can. J. Phys., 58(1980) 1200-11*

[12] *J. C. Slater, The Self-Consistent Field for Molecular and Solids, Quantum Theory of Molecular and Solids, Vol. 4 (McGraw-Hill, New York, 1974).*

1.4. Basis sets

Nowadays, computational chemistry calculations are performed within a set of basis functions[13]. In these case, the wave-functions under consideration are all represented depending of the adjustment.

Basis sets were developed by J.C. Slater, who fit atomic orbitals by means of simpler functions to facilitate the calculations. As a consequence, basis sets incorporate only a limited number of functions, called Slater orbitals (see eq. 8). These Slater Type Orbital (STO), keep the same dependence with the exponential of the radius found in the hydrogen orbitals:

$$STO = \frac{\xi^3}{\pi^{\frac{1}{2}}} \cdot e^{(-\xi * r)} \qquad (8)$$

Later on, Frank Boys realized that STOs could in turn be approximated as a linear combination of Gaussian functions (GTO, see eq. 9), which allow a faster calculation of the molecular integrals:

$$GTO = \frac{2\chi}{\pi^{\frac{3}{4}}} \cdot e^{(-\chi * r^2)} \qquad (9)$$

All basis set[14] equations based in Slater Type Orbital (STO) are considered minimal basis set. The current form of STO is STO-nG where n value represents the number of Gaussian primitive function comprising a single basis function. In this type of basis sets exists the same number of Gaussian primitives comprising the core and the valence orbitals. The most common STO-nG are; STO-3G, STO-6G, STO-3G* and STO-6G*. The last pair are the polarized version of STO-3G and STO-6G respectively.

[13] *Errol G. Lewars. Computational Chemistry: Introduction to the Theory and Applications of Molecular and Quantum Mechanics (1st ed.). Springer.*
[14] *Jensen, Frank (2013). "Atomic orbital basis sets". WIREs Comput. Mol. Sci. 3: 273–295.*

Nowadays, there are additional types of extended basis sets:

Double-Zeta, Triple-Zeta and Quadruple-Zeta: The double-zeta is important because allows to treat each orbital separately when it conducts the H-F calculations. Moreover, this leads to a more accurate representation of each orbital. The triple and quadruple-zeta basis sets work similar, except that they use three and four Salter equations instead of two.

Split-Valence basis set: Often takes too much effort to calculate a *double-zeta* for every orbital. This can be simplified calculating a double-zeta only for the valence orbital. Since the electrons of the inner-shell (core shell) are not usually involved in chemical reactivity or bond formation, they can be described using a single STO. The most common split-valence sets are 3-21G, 4-31G and 6-31G. As can be seen in *Figure 3* each part of the nomenclature has a meaning.

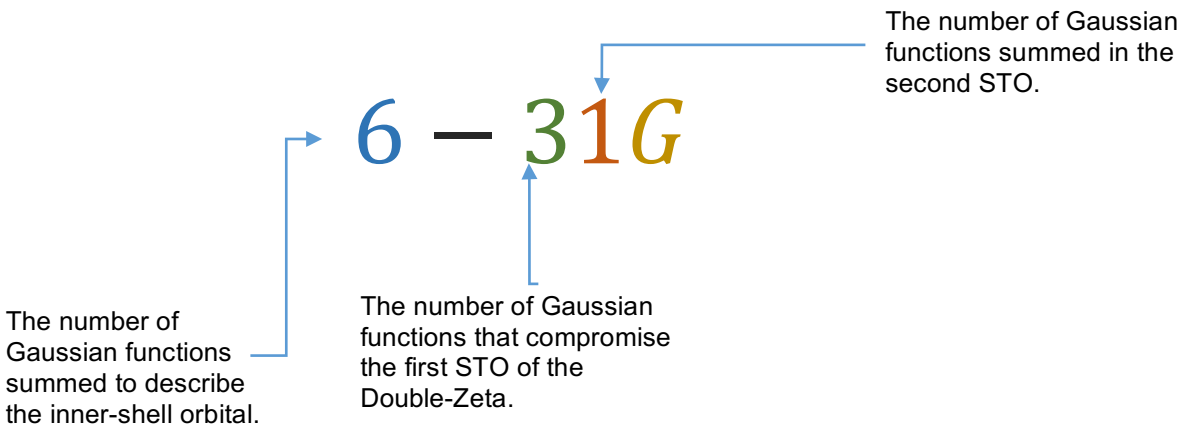

Figure 3: Explicative scheme of nomenclature of Split-Valence basis set.

Polarization functions: The basis sets that have been presented before only describe occupied atomic. Polarized basis sets incorporate functions to atoms with higher angular momenta than required for the description of the ground state.

When the representation has one asterisk at the end of a basis set this means that polarization has been taken into account in the *d* orbital for heavy atoms, meanwhile two asterisks denotes that the polarization provides additional *p* orbitals for hydrogen atoms (see *Figure 4*).

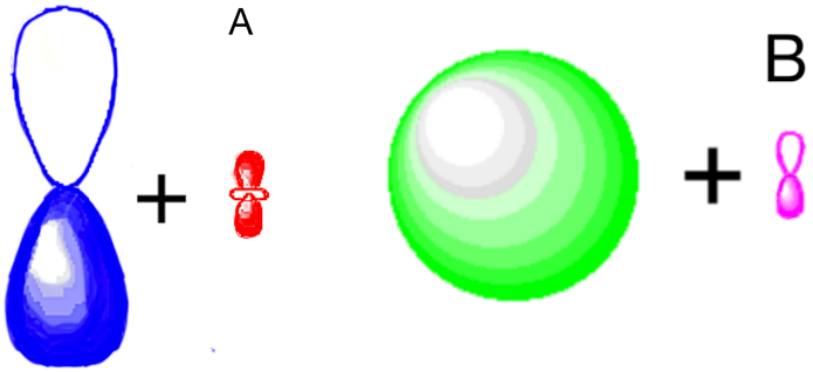

Figure 4:A) It is represented the basis 6-31G. It is composed by an orbital p (Blue) and a little orbital d (red). B) Picture b is the basis 6-31G** which is composed by ab orbital s (green) and a little orbital p (pink).*

1.5. Density Functional based Tight Binding (DFTB)

The Density Functional based Tight Binding method is based on the expansion of the DFT Kohn-Sham total energy with respect to a small charge density fluctuation. In the last years, the use of DFTB[15] method has increased since allows the calculation of large molecular systems, or even the optical excited state properties.

Developing the *eq. 2* in terms of the orbitals:

$$E = \sum_i n_i \left\langle \psi_i \left| -\frac{1}{2}\nabla^2 + V_{ext} + \frac{1}{2}\int \frac{\rho(r')}{|r-r'|} dr' \right| \psi_i \right\rangle + E_{XC}[\rho(r)] + E_{nuc}(R) \qquad (10)$$

If we perform a second expansion of Taylor series[16], with respect to the reference density[17] ρ_o.

$$\rho(r) \approx \rho_o(r) + \delta\rho_o(r) \qquad (11)$$

[15] Koskinen, P.; Mäkinen, V. Computational Materials Science 47 (2009) 237
[16] Elstner, M.; Seifert, G. Philosophical Transactions of the Royal Society A 372 (2012) 483
[17] Porezag, D.; Frauenheim, Th.; Kohler, Th.; Seifert, G.; Elstner, M. Physical Review B 51 (1995) 12947

the new expression is:

$$E = \sum_i n_i \left\langle \psi_i \left| -\frac{1}{2}\nabla^2 + V_{ext} + \frac{1}{2}\int \frac{\rho_o(r')}{|r-r'|}dr' + V_{XC}[\rho_o(r)] \right| \psi_i \right\rangle - \frac{1}{2}\int\int \frac{\rho_o(r')\big(\rho_o(r)+\delta\rho_o(r)\big)}{|r-r'|}dr'dr - \int V_{XC}[\rho_o(r)]\big(\rho_o(r)+\delta\rho_o(r)\big)dr + E_{XC}[\rho_o(r)+\delta\rho_o(r)] + E_{nuc}(R) \quad (12)$$

where $E_{nuc}(R)$ also incorporates terms associated with pseudo-potentials, which simulate the core electrons, and thus allowing to use only the electrons of the valence layers. Thus rearranging previous equation:

$$E = \sum_i n_i \langle \psi_i | \hat{H}_o | \psi_i \rangle + \frac{1}{2}\int\int \left(\frac{1}{|r-r'|} + \left. \frac{\delta^2 E_{XC}}{\delta\rho_o(r)\delta\rho_o(r')} \right|_{\rho_o} \right) \delta\rho_o(r)\delta\rho_o(r')dr'dr$$

$$+ \left(-\frac{1}{2}\int\int \frac{\rho_o(r')\rho_o(r)}{|r-r'|}dr'dr + E_{XC}[\rho_o(r)] - \int V_{XC}[\rho_o(r)]\rho_o(r)dr + E_{core} \right) \quad (13)$$

The equation can be reduced to:

$$E[\rho, \delta\rho] = \sum_i n_i \langle \psi_i | \hat{H}_o | \psi_i \rangle + E_{Rep}[\rho, \delta\rho] + E_{Coul}[\rho, \delta\rho] \quad (14)$$

where the repulsive and Coulombic terms are usually approximated to simpler expressions:

$$E_{Rep}[\rho,\delta\rho] = \left(-\frac{1}{2}\int\int\frac{\rho_o(r')\rho_o(r)}{|r-r'|}dr'dr + E_{XC}[\rho_o(r)] - \int V_{XC}[\rho_o(r)]\rho_o(r)dr + E_{core}\right)$$

$$\approx \sum_i\sum_j V_{Rep}^{i,j}(R_{i,j}) \tag{15}$$

In *eq. 15*, each pair of atoms *i,j* have a repulsive function $V_{Rep}^{i,j}$ depending only on the atomic types, which is obtained by fitting high level theoretical calculations.

$$E_{Coul}[\rho,\delta\rho] = \frac{1}{2}\int\int\left(\frac{1}{|r-r'|} + \frac{\delta^2 E_{XC}}{\delta\rho_o(r)\delta\rho_o(r')}\bigg|_{\rho_o}\right)\delta\rho_o(r)\delta\rho_o(r')dr'dr$$

$$\approx \frac{1}{2}\sum_i\sum_j \gamma_{i,j}(R_{i,j})\Delta q_i\Delta q_j \tag{16}$$

where, γ_{ii} is a parameter that depends on factors such as the ionization energy and the electroafinity; and the extra electron population of the atom, Δq_i, is obtained from the fluctuation of the electron density, $\delta\rho(r)$, within the atomic volumen:

$$\Delta q_i \approx \int_{Vol_i}\delta\rho(r)dr \tag{17}$$

additionally, the density fluctuation is obtained from the extra electron populations:

$$\delta\rho(r) = \sum_i \Delta q_i\delta\rho_i(r) \tag{18}$$

Thus, due to this relationship, both the variation of charge and density ($\Delta q_i, \delta\rho$) must be obtained in a self-consistent way.

1.5.1. Basis sets and functional types.

Since we consider only valence electrons, the repulsive energy must simulate all the effects arising from the inner core electron. Moreover, given that the tight-binding assumes tightly bound electrons, we use minimal local basis in the LCAO expansion:

$$\psi_i(r) = \sum_{\mu} c_{i,\mu}\phi_{\mu}(r) \tag{19}$$

This means having only one radial function for s-states, three for p-states, and so on. Also, real spherical harmonics are used.

On the other hand, regarding the type of functionals, DFTB makes use of the LDA approximation (for both the free and pseudo-atom). Despite more recent xc-functionals could be used, they do not improve DFTB parametrizations, whereas LDA provides a fixed level of theory to build foundation. However, this is not true for the repulsive potential fitting, for which more accurate DFT functionals can–and should be–used.

2. OBJECTIVES

2. OBJECTIVES

Graphene has generated excitement due to its unusual properties. In present work we will study the graphene absorbance containing PEG, among other functional groups, on the surface. We will use quantum mechanics method to study this propriety, however it will be necessary to validate the correct method.

To sum up, there are two main objectives:

1: Validate the correct Quantum mechanical method with different sizes of graphene structures and different functional groups.

2: Compare, for the selected method, the absorbance property of graphene with different functional groups, such as: ***-NH_2***, ***-OH***, ***-CHO*** and ***PEG-200***.

3. VALIDATION

3. VALIDATION

In this section, the appropriate method for investigating various substituents on graphene sheets will be chosen. Since the size of the sheets is of the order of several nm, we will need to use semi-empirical methods such as **DFTB** or **AM1** (Austin Model 1).

For this purpose, we will perform a comparison of both methods against much more accurate ones, such as: **BLYP**, **BPBE** and **B3LYP**. In this case, there are two GGA based methods (BLYP and BPBE) and a hybrid GGA one (B3LYP), which are widely used in computational chemistry, for smaller systems.

Indeed, the results of the queries for the keywords DFT and B3LYP, in two of the main research editorials[18] [19], are shown in *Graphic 1*. These results exhibit that: i) DFT methods are widely used in computational chemistry research, and ii) albeit new xc-functionals are in constant development (such as hybrid meta-GGA M06), B3LYP is still extensively used. Thus, this last functional will be used as the reference method in our work.

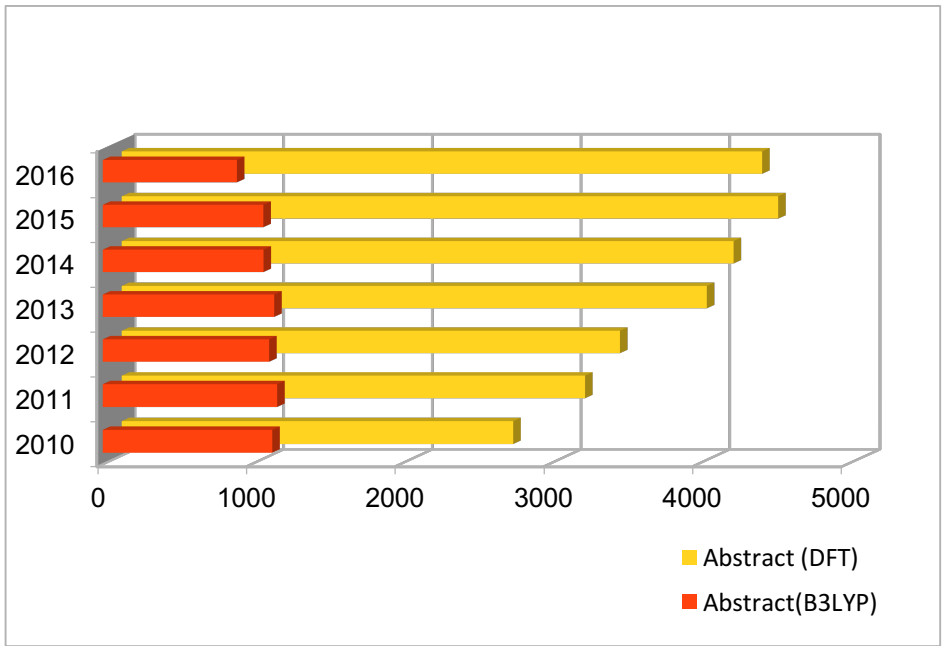

Graphic 1: Publications per year from 2010 to 2016 containing DFT in the abstract and those containing B3LYP with respect to the previous one. Contrast data from ACS and Science Direct editorials.

[18] Pubs.acs.org. (2017). ACS Publications Home Page. [online] Available at: http://pubs.acs.org [Accessed 19 April 2017]
[19] Sciencedirect.com. (2017). ScienceDirect.com | Science, health and medical journals, full text articles and books.. [online] Available at: http://www.sciencedirect.com [Accessed 26 Jun. 2017].

The validation process starts with the optimization of geometries of different molecules for each selected method. The results we will focus on are:

1) Average of distances **Csp^2- Csp^2**.
2) Homo - Lumo gap value **(ΔE_{L-H}).**

The starting geometries needed for the optimizations were generated with the help of the Jmol[20] software. Each graphene sheet was given a nomenclature based on the number of rings involved in the radius, thus resulting in 1R, 2R and 3R. In *Figure 5* a scheme of each nomenclature can be observed. It is important to recall that all geometries have been optimized for each of the selected methods.

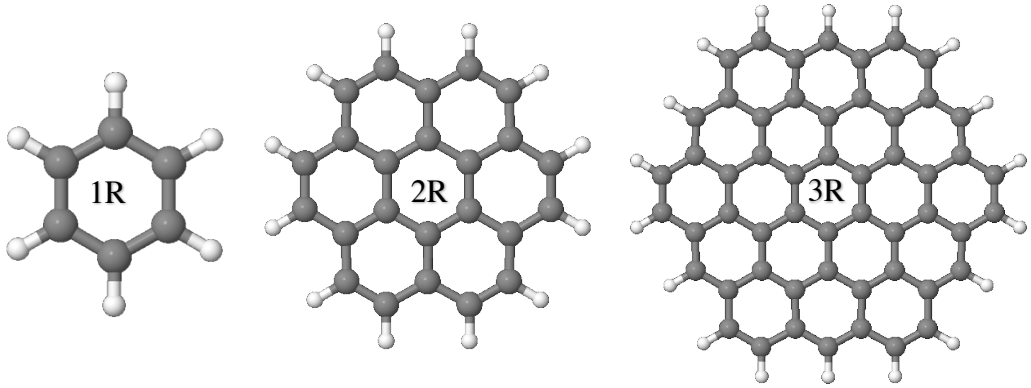

Figure 5: Explanatory scheme of the type of nomenclature used throughout the investigation

We use the Gaussian-09[21] program for BLYP, B3LYP, BPBE and AM1 methods, and the DFTB+[22] (with mio-1-1[23] set of parameters) for the DFTB calculations. The different results obtained are shown in *Table 1* (1R), *Table 2* (2R) and *Table 3* (3R).

[20] *mol.sourceforge.net. (2017). Jmol: an open-source browser-based HTML5 viewer and stand-alone Java viewer for chemical structures in 3D. [online] Available at: http://jmol.sourceforge.net [Accessed 24 Apr. 2017].*

[21] *M. J. Frisch, G. W. Trucks, H. B. Schlegel, G. E. Scuseria, M. A. Robb, J. R. Cheeseman, G. Scalmani, V. Barone, B. Mennucci, G. A. Petersson, H. Nakatsuji, M. Caricato, X. Li, H. P. Hratchian, A. F. Izmaylov, J. Bloino, G. Zheng, J. L. Sonnenberg, M. Hada, M. Ehara, K. Toyota, R. Fukuda, J. Hasegawa, M. Ishida, T. Nakajima, Y. Honda, O. Kitao, H. Nakai, T. Vreven, J. A. Montgomery, Jr., J. E. Peralta, F. Ogliaro, M. Bearpark, J. J. Heyd, E. Brothers, K. N. Kudin, V. N. Staroverov, R. Kobayashi, J. Normand, K. Raghavachari, A. Rendell, J. C. Burant, S. S. Iyengar, J. Tomasi, M. Cossi, N. Rega, J. M. Millam, M. Klene, J. E. Knox, J. B. Cross, V. Bakken, C. Adamo, J. Jaramillo, R. Gomperts, R. E. Stratmann, O. Yazyev, A. J. Austin, R. Cammi, C. Pomelli, J. W. Ochterski, R. L. Martin, K. Morokuma, V. G. Zakrzewski, G. A. Voth, P. Salvador, J. J. Dannenberg, S. Dapprich, A. D. Daniels, Ö. Farkas, J. B. Foresman, J. V. Ortiz, J. Cioslowski, and D. J. Fox, Gaussian 09 (Gaussian, Inc., Wallingford CT, 2009).*

[22] *B. Aradi, B. Hourahine, and Th. Frauenheim. DFTB+, a sparse matrix-based implementation of the DFTB method. J. Phys. Chem. A, 111(26):5678, 2007.*

[23] *Dftb.org. (2017). mio-1-1 CC. [online] Available at: https://www.dftb.org/parameters/download/mio/mio-1-1-cc/ [Accessed 7 May 2017].*

1R

Method	Homo	Lumo	Δ (kcal/mol)	dst(C,C)
BLYP	-0,2083	-0,0195	118,45	1,407
BPBE	-0,2177	-0,0266	119,89	1,404
B3LYP	-0,2463	0,0036	156,80	1,397
AM1	-0,3547	0,0204	235,39	1,395
DFTB	-0,2462	-0,0514	122,23	1,396

Table 1: Data of calculations using different methods for 1R.

2R

Method	Homo	Lumo	Δ (kcal/mol)	dst(C,C)
BLYP	-0,1710	-0,0667	65,44	1,424
BPBE	-0,1810	-0,0756	66,19	1,420
B3LYP	-0,2003	-0,0520	93,01	1,414
AM1	-0,3009	-0,0360	166,18	1,412
DFTB	-0,2098	-0,1040	66,39	1,416

Table 2: Data of calculations using different methods for 2R.

3R

Method	Homo	Lumo	Δ (kcal/mol)	dst(C,C)
BLYP	-0,1565	-0,0875	43,26	1,428
BPBE	-0,1670	-0,0973	43,72	1,424
B3LYP	-0,1813	-0,0776	65,08	1,418
AM1	-0,2773	-0,0664	132,37	1,416
DFTB	-0,1947	-0,12569005	43,30	1,420

Table 3: Data of calculations using different methods for 3R.

As can be deduced from the tables, both BLYP and BPBE provide very similar results. The reason is because both are GGA type functionals. When they are compared to B3LYP, both gives raise too lower ΔE_{L-H} values, but longer Csp2- Csp2 bond distances.

Regarding the semi-empirical methods, the geometries obtained by means of the AM1 Hamiltonian are closer to the B3LYP ones, but the ΔE_{L-H} values are too high. Finally, the DFTB methodology provides data really close to BLYP and BPBE, while the geometries are similar to those obtained with the B3LYP functional.

As mentioned in the introduction, the foundations of the DFTB methodology are based on the LDA approximation, but in the last versions it has been corrected introducing terms of GGA. This is the reason why the energetic results obtained from DFTB are very similar to BLYP or BPBE. Moreover, B3LYP calculations have been incorporated in the last parametrizations, thus providing higher accuracy in the geometries, and better values of the ΔE_{L-H} gaps.

Taking all the above into account, DFTB will be the chosen methodology to perform present study, since AM1 provides higher values of ΔE_{L-H} for all sheets. Ideally, we should use the B3LYP functional, but it is actually prohibitive due to the CPU time that would require to perform calculations on larger sheets of graphene.

4. RESULTS

4. RESULTS

As can be derived from the previous section, the method to carry out our investigation will be DFTB, since it provides the best results compared to the amount of resources needed to perform the calculations.

The values of the HOMO-LUMO gap, after performing the optimization of different graphene sheets (sizes ranging from 1 to 16R), are displayed in the *Table 4*. It is important to emphasize the tendency of this gap with the sheet size. In addition, the size (in Å) and the value of the wavelength for each absorption (in nm) are also displayed.

R	nC	ndst	ΔE_{L-H} (DFTB)	siz (Å)	λ (nm)
1	6	6	122,23	2,47	234
2	24	30	66,39	7,40	431
3	54	72	43,30	12,33	660
4	96	132	30,14	17,27	949
5	150	210	21,39	22,20	1337
6	216	306	15,16	27,13	1885
7	294	420	10,62	32,06	2693
8	384	552	7,31	37,00	3914
9	486	702	4,93	41,93	5794
10	600	870	3,28	46,86	8722
11	726	1056	2,14	51,80	13347
12	864	1260	1,37	56,73	20823
13	1014	1482	0,82	61,66	35012
14	1176	1722	0,45	66,59	63300
15	1350	1980	0,21	71,53	138829
16	1536	2256	0,04	76,46	724270

Table 4: Results obtained by the DFTB method, where; nC is the number of carbons; ndst is the number of distances between C-C; ΔEL-H is the difference between Lumo-Homo; size means diameter length. λ is the value for the absorption.

When the HOMO-LUMO difference is represented vs the size of the ring (in Å), we observe that the gap decreases when the carbon sheet increases, until it becomes practically inexistent. This is a logical consequence since Graphene is, actually, a conductor. Nevertheless, it should be noted that the barriers obtained with DFTB are underestimated, as has been previously demonstrated in *section 3*.

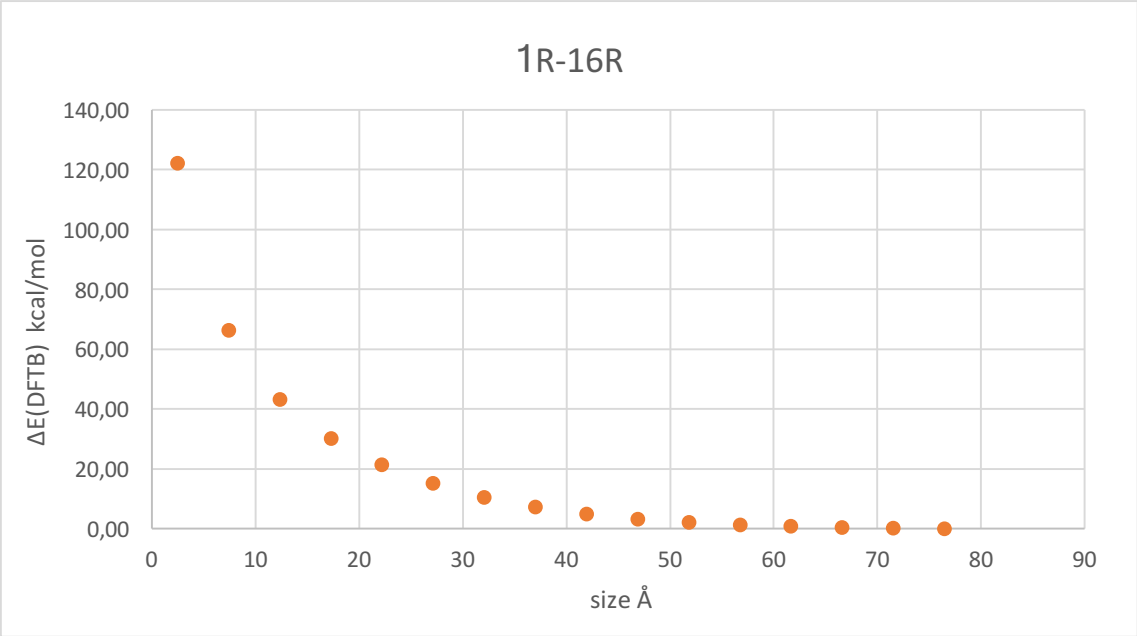

Graphic 2: Representation of ΔE_{L-H} in front of size. It can be observed the decrease of the energy.

Interestingly, the obtained results are in good agreement with the experimental ones reported in the bibliography[24]. Indeed, Xiong[25] and his coworkers have measured values for the absorbance in a range **780 - 1760 nm**, for the case of nano-sheets of graphene sized between **1.7 and 2.7 nm**. These sizes would correspond to our **4R – 6R** models, for which we have obtained absorbance values in the interval **950 – 1900 nm**.

[24] *Liu, Q., Guo, B., Rao, Z., Zhang, B. and Gong, J. (2013). Strong Two-Photon-Induced Fluorescence from Photostable, Biocompatible Nitrogen-Doped Graphene Quantumots for Cellular and Deep-Tissue Imaging. Nano Letters, 13(6), pp.2436-2441.*

[25] *Xiong, F., Zhang, J., Zhu, Z., Yuan, X. and Qin, S. (2015). Ultrabroadband, More than One Order Absorption Enhancement in Graphene with Plasmonic Light Trapping. Scientific Reports, 5(1).*

4.1. Functional Groups

One of the objectives of the work is to study the effect of different substituents, in the form of different functional groups. The aim is to understand the relationship between the kind of functional group and its effect on the HOMO-LUMO gap; thus explaining the changes induced in the optical properties such as fluorescence or absorbance.

The study has been performed on the three different sheet sizes (4 - 6R), and with several functional groups and arrangements: Clean (without functional group), *CHO* (single substitution), *fCHO* ("filled"), NH_2 (single), fNH_2 ("filled"), *OH* (single), *fOH* ("filled"), *PEG* (single), *fPEG* and *rPEG*[26] (both "filled"). The "filled" substitution has been carried out by introducing a functional group on every 3 carbons, in order to avoid overlaps, as can be noted in *Figure 8*. For the shake of simplicity, a brief overview of the nomenclature is presented in *Table 5*.

Nomenclature	F.Group	Description
Clean	----------	Without functional group
CHO	aldehide	Only one
fCHO	aldehide	Each 3 hydrogens, one CHO
OH	alcohol	Only one
fOH	alcohol	Each 3 hydrogens, one OH
NH_2	ammonia	Only one NH2
fNH_2	ammonia	Each 3 hydrogens, one NH2
PEG	PEG-200	Only one linear PEG-200
fPEG	PEG-200	Each 3 hydrogens, one linear PEG-200
rPEG	PEG-200	Each 3 hydrogens, one PEG-200

Table 5: Scheme of the nomenclature and visual examples. The examples with the name NONE just are following the same structure than the others.

[26] *Li, Y., Shu, H., Niu, X. and Wang, J. (2015). Electronic and Optical Properties of Edge-Functionalized Graphene Quantum Dots and the Underlying Mechanism. The Journal of Physical Chemistry C, 119(44), pp.24950-24957.*

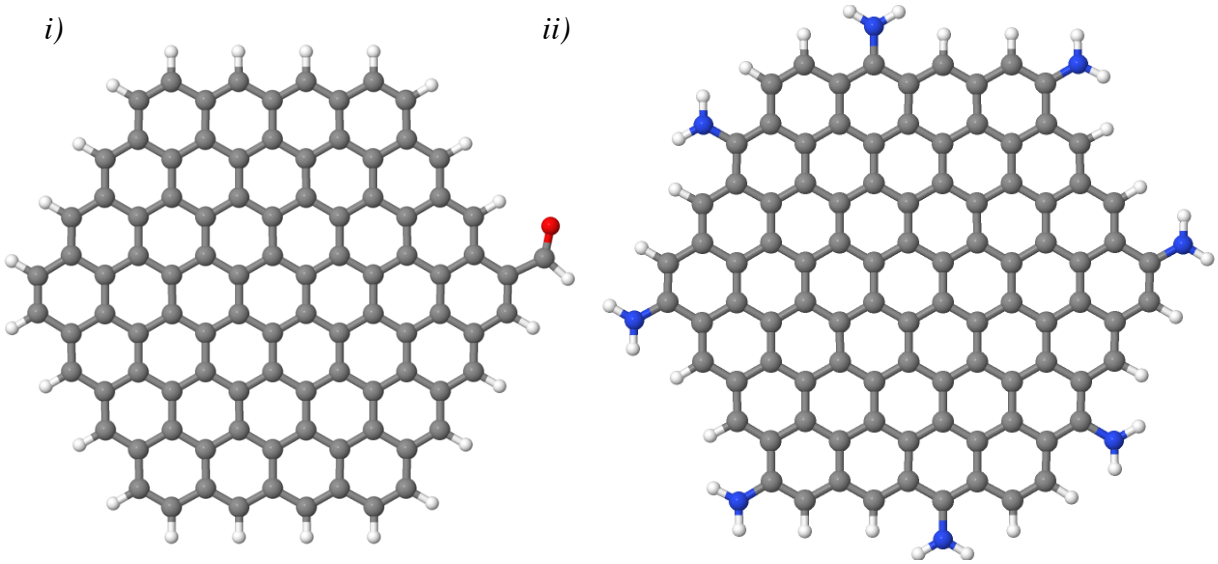

Figure 6: i) 4R graphene sheet with only one substitution of –CH0. 4R-OH. ii) 4R graphene sheet filled with -NH_2 substitutions. 4R-fNH_2.

4.1.1. 4R sheet

The energies of the HOMO and LUMO orbitals for each substitution in the a 4R graphene sheet have been obtained, after a geometry optimization of each model using the DFTB method, as shown in *Table 6*.

F. Group	HOMO(Ha)	LUMO(Ha)	ΔE_{L-H} (kcal/mol)
Clean	-0,186	-0,138	30,1
CHO	-0,188	-0,142	29,1
NH2	-0,180	-0,136	28,1
OH	-0,185	-0,138	29,3
PEG	-0,184	-0,137	29,3
fCHO	-0,210	-0,170	25,0
fNH2	-0,143	-0,110	20,7
fOH	-0,166	-0,128	23,7
fPEG	-0,177	-0,133	27,6
rPEG	-0,169	-0,126	26,8

Table 6:Data of orbital energies for each functional group in a 4R graphene sheet.

If we represent the data in a graphical form, it can be noticed that the lowest ΔE_{L-H} corresponds to the fNH2 substitution. In addition, no significant change is noticed between the fPEG and rPEG groups, but both largely differ from fOH, although this is not happening with the single substitutions (OH and PEG). This would mean that both OH and PEG have the same effect when they are alone. The reason could be that the

PEG is bound through an ether group to the graphene ring, giving rise to a similar behavior than the alcohol group. Nevertheless, this is no longer observed when the sheet contains more than one PEG or OH.

With regard to the HOMO position, a great variation for the fCHO and fNH_2 is observed, as can be seen in *Graphic 3*. In the case of the fCHO, the energy largely diminishes, while in fNH_2 increases. This fact could be important in the manufacture of interfaces between conductors.

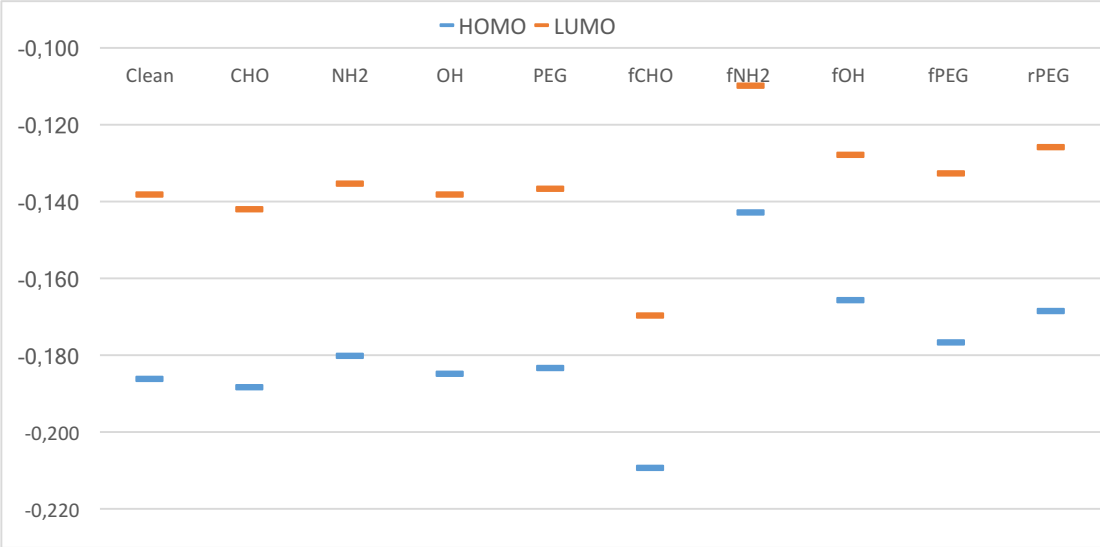

Graphic 3:Representation of the energies for a 4R graphene sheet. Axis Y in Ha.

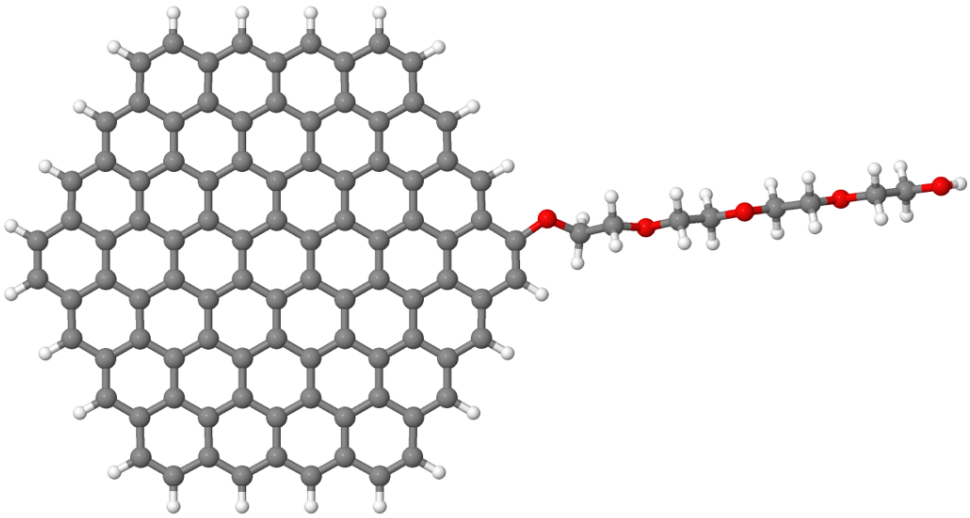

Figure 7: Example of monosubstitution with PEG-200.

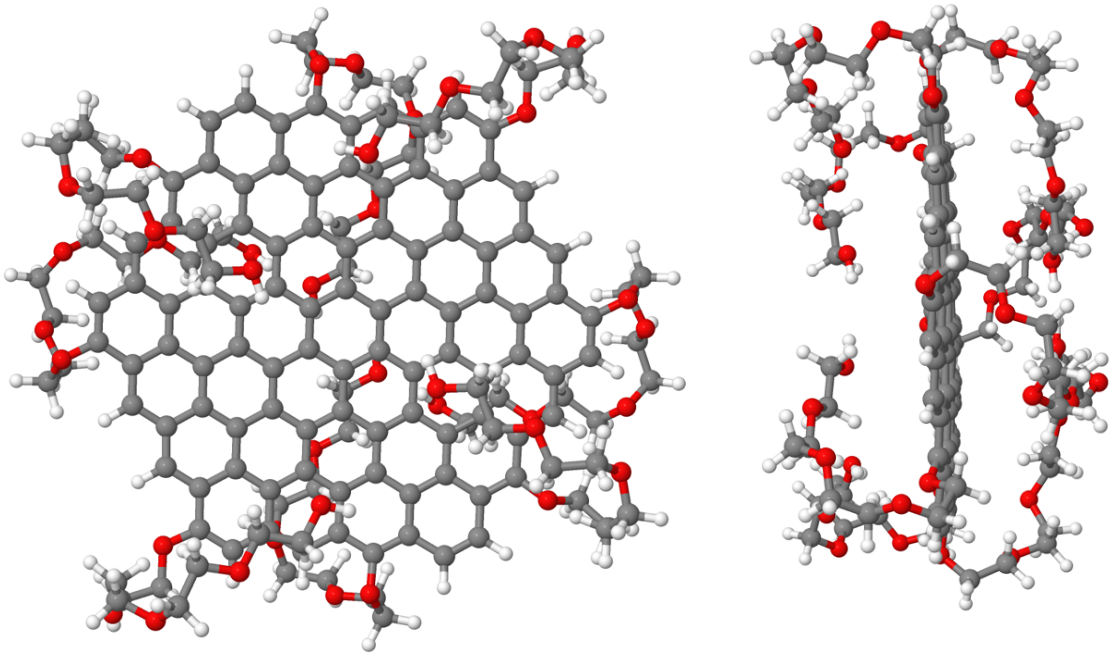

Figure 8: Example of complete replacement with rPEG-200 from different perspectives

4.1.2. 5R sheet

Just as before, the same procedure is performed for the 5R graphene sheet *(Figure 9)*, being the results reported on *Table 7*.

F. Group	HOMO (Ha)	LUMO (Ha)	ΔE_{L-H} (Kcl/mol)
Clean	-0,181	-0,147	21,4
CHO	-0,182	-0,149	20,8
NH2	-0,177	-0,145	20,3
OH	-0,180	-0,147	20,8
PEG	-0,179	-0,146	21,0
fCHO	-0,203	-0,173	18,8
fNH2	-0,144	-0,118	16,4
fOH	-0,164	-0,135	18,6
fPEG	-0,173	-0,140	20,5
rPEG	-0,162	-0,130	19,7

Table 7: Data of orbital energies for each functional group in a 5R graphene sheet.

As discussed before for 4R, both PEG and OH show the same trend on single substitutions, which is broken in the fPEG or rPEG with respect to fOH, but with a lower deviation than before. Indeed, fOH still provides the lowest ΔE_{L-H} gap of these kind of groups.

Again, the lowest band gap belongs to fNH_2 (see *Graphic 4*), having a similar value for the HOMO energy. If we focus on the gaps for fCHO and fOH, it can be seen that they decrease in the 5R regarding to the 4R.

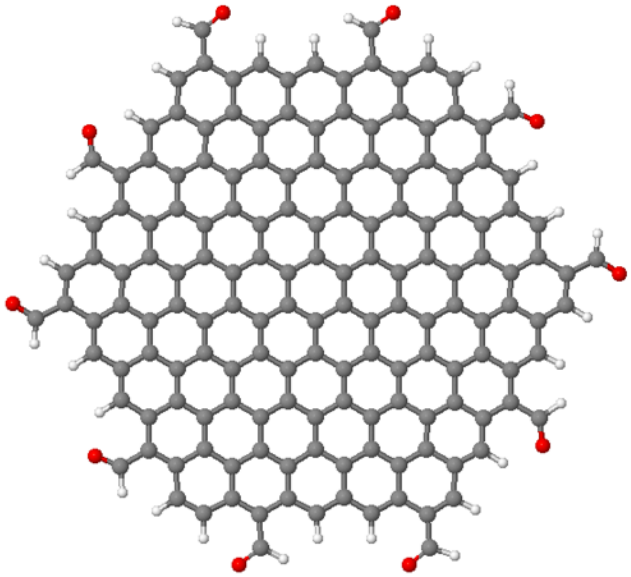

Figure 9: 5R graphene sheet filled with -COH groups.

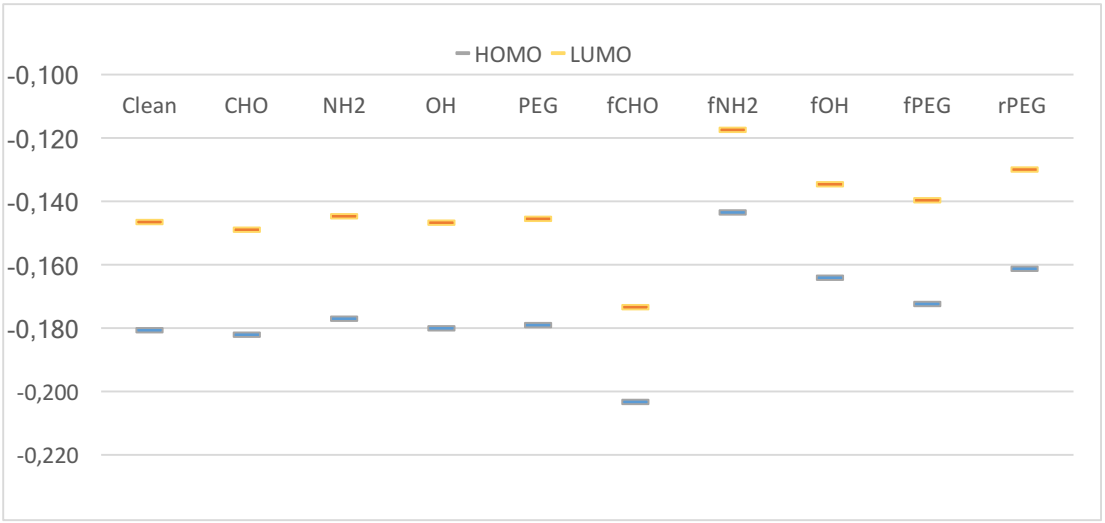

Graphic 4: Representation of the energies for a 5R graphene sheet. Axis Y in Ha.

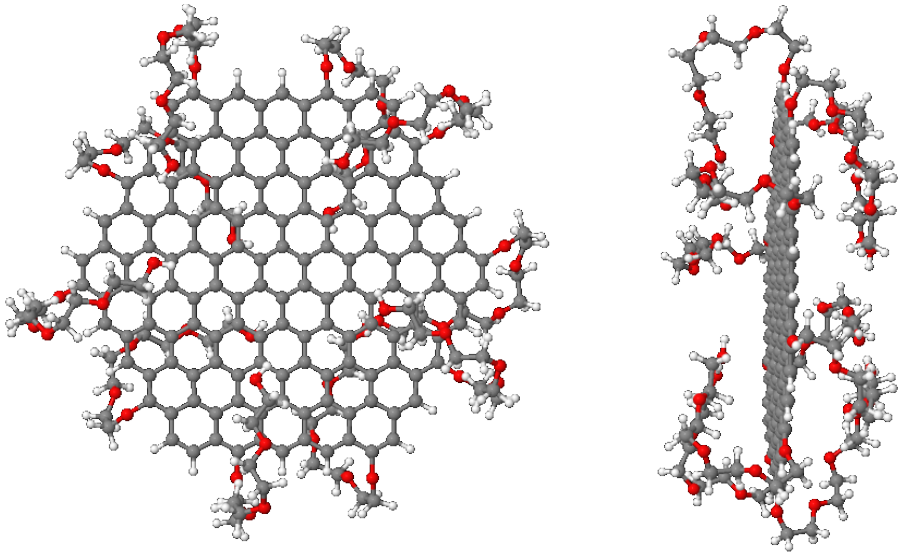

Figure 10: 5R graphene sheet with rPEG-200.

4.1.3. 6R sheet

Following the trend of the previous sections, the effect of the single substitutions for each functional group are becoming smaller as the size of the nanoparticle increases.

This is the reason why in this section monosubstitutions have been obviated, since their effect was already minimal in 4R and 5R. In any case, to make sure that single substitutions are not significant on larger sheets, a small benchmark has been carried out, as can be seen on *Table 8*.

R	OH:Δ(L-H) Kcal/mol	PEG:Δ(L-H) Kcal/mol	CHO:Δ(L-H) Kcal/mol	NH2:Δ(L-H) Kcal/mol
7	8,54	9,76	8,82	7,48
8	6,35	7,03	6,22	5,63
9	4,23	4,70	4,14	3,62
10	2,55	3,03	2,56	2,01
11	1,70	2,03	1,52	1,14

Table 8: Check that the effect of the monosubstitution is minimal

As done before, the clean and the different "filled" substitutions have been optimized for the 6R sheet, and the data obtained is presented in *Table 9*. Again, the different data is also reported in a graphical form in *Graphic 5*.

F. Group	HOMO (Ha)	LUMO (Ha)	ΔE_{L-H}(kcal/mol)
Clean	-0,177	-0,153	15,2
fCHO	-0,201	-0,179	13,6
fNH2	-0,142	-0,121	13,3
fOH	-0,159	-0,137	14,0
fPEG	-0,163	-0,140	14,7
rPEG	-0,162	-0,139	14,3

Table 9:Data of orbital energies for each functional group in a 6R graphene sheet.

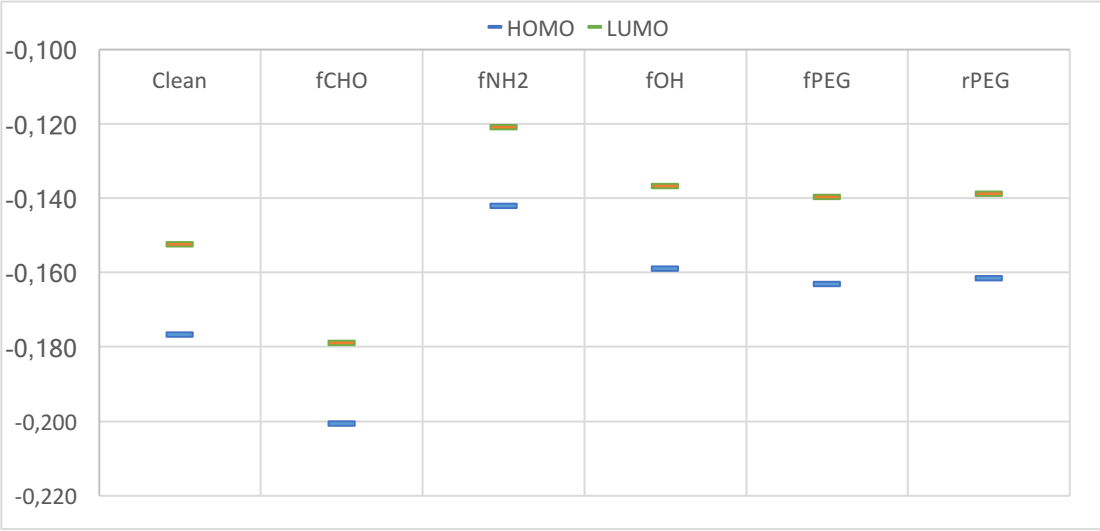

Graphic 5:Representation of the energies for a 4R graphene sheet. Excluding monosubstitutions. Axis Y in Ha.

These results clearly show that the larger the size of the graphene sheet, the smaller the effects of the functional groups. Hence, in *Graphic 5* it can be observed that now the energies are not so different as in the other nanoparticles. The explanation can be inferred from the sequence of pictures shown in *Figure 11*, where the models from 4R to 8R and 10R are represented when the PEG, the largest substituent, is used. Thus, it is easy to realize that rPEG becomes insignificant as the size of the ring increases.

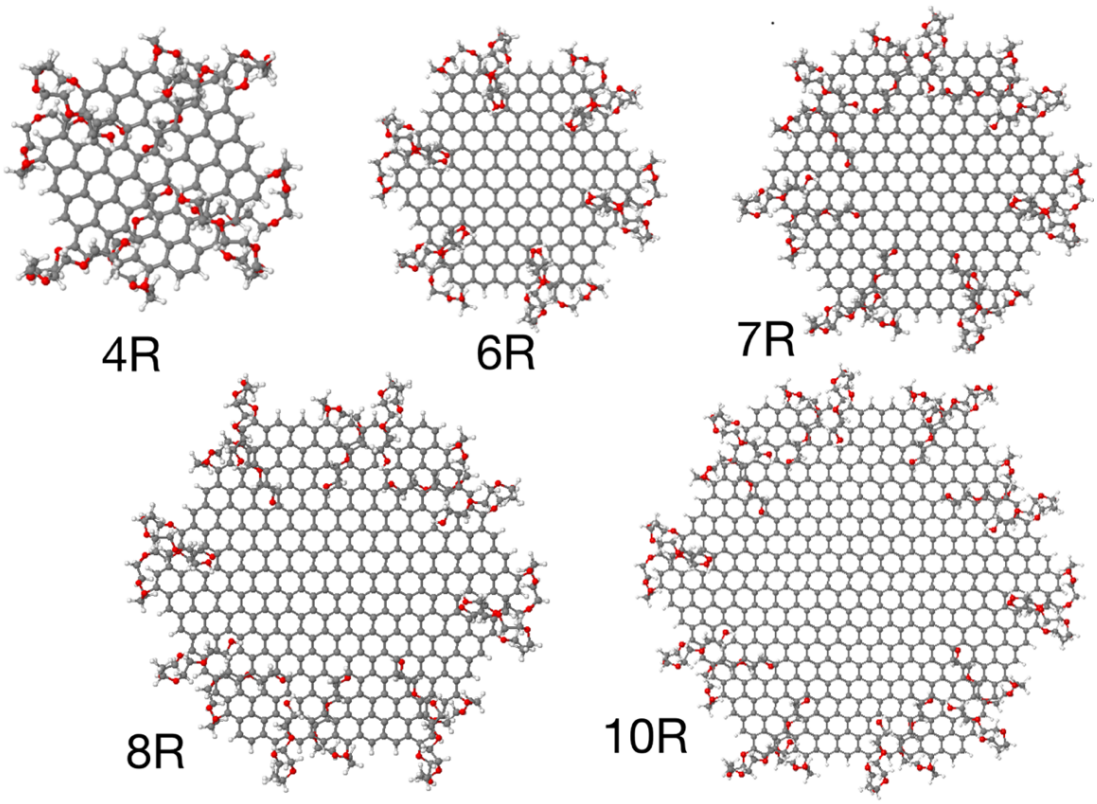

Figure 11: Sequence of increasing sizes of rPEG.

In this point it is noteworthy to recall the results presented in the *Graphic 2*, where it was shown that the HOMO-LUMO gap decreases with the sheet size, being the 6R close to the turning point.

5. CONCLUSION

5. CONCLUSIONS

All conclusions of the different sections (*4.1.1, 4.1.2 and 4.1.3*) will be presented in common. Using the same data tables, the *Graphic 6* shows that -NH2 filled have the highest HOMO-LUMO energy difference, while the fCHO has the lowest one. The performance of –OH and –PEG are similar in all sheets with the different substitutions when the size of sheet increases the ΔE_{L-H} decreases, even so the PEG-200 shows huge improvement in the optical activity. All these results are showed in the *Graphic 6*.

In addition, if *Graphic 7* is analysed in detail it can be observed that –NH2 the LUMOs practically do not vary in the NH_2 substitution, as it has been named in the previous sections.

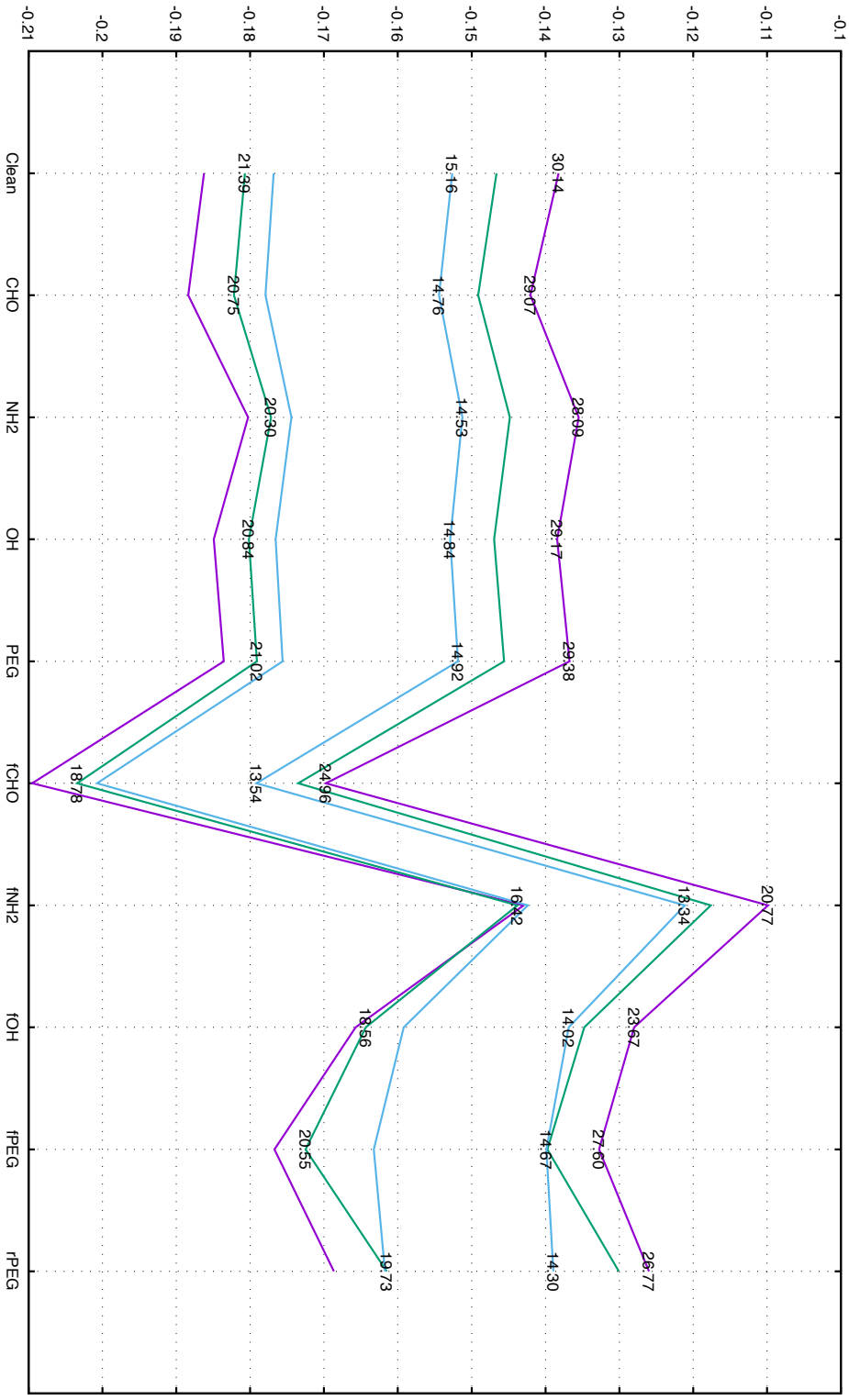

Graphic 6: Representation of HOMO and LUMO levels for Graphene sheets of 4R, 5R and 6R. The numbers belong to ΔE_{L-H} (kcal/mol). Axis Y in Ha.

This fact had led us to make *Graphic 7* where the HOMOs are compared each substitution vs the number of carbons.

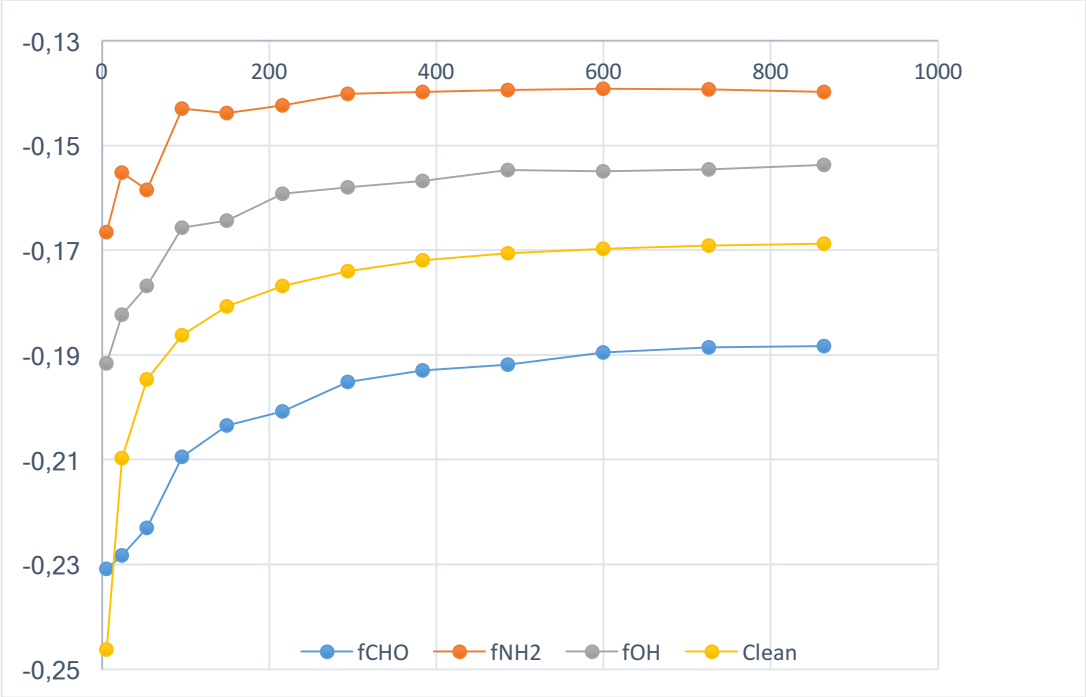

Graphic 7: HOMOs vs nC of substitutions. Axis Y in Ha.

After analysing *Graphic 7*, we can say that substitution fNH_2 normalizes the HOMO to a size close to 96 carbons, which would correspond to a 4R sheet. From this value, the HOMO strip will remain constant. Also, the other substituents will be affected in the same way however in larger size. The one that takes longer to normalize is the fCHO, which for the studied sheets no constant value has been observed.

The effect of the different functional groups on the graphene nanoparticles has been our objective. We decided to focus only on the 4R, 5R and 6R sizes due to the experimental results reported in the bibliography. Furthermore, a summary of the absorbance obtained for each size and substituent is presented in *Table 10*, with the aim to assist experimental researchers.

	λ4R(nm)	λ5R(nm)	λ6R (nm)
Clean	949	1337	1883
CHO filled	1145	1523	2107
NH2 filled	1378	1746	2149
OH filled	1208	1540	2040
PEG filled	1036	1392	1950
rPEG filled	1068	1449	1999

Table 10: Absorbance of the different graphene sheets. Measured in nm.

With the calculated absorbance we can state that, for the studied sizes, they are in the near-IR with a range in **800 - 2500**[27] nm.

[27] En.wikipedia.org. (2017). *Infrared*. [online] Available at: https://en.wikipedia.org/wiki/Infrared [Accessed 12 May 2017].

6. ATTACHMENTS

6. ATTACHMENTS

6.1. EXAMPLE OF LINEAR PEG-200 IN A SHEET 10R.

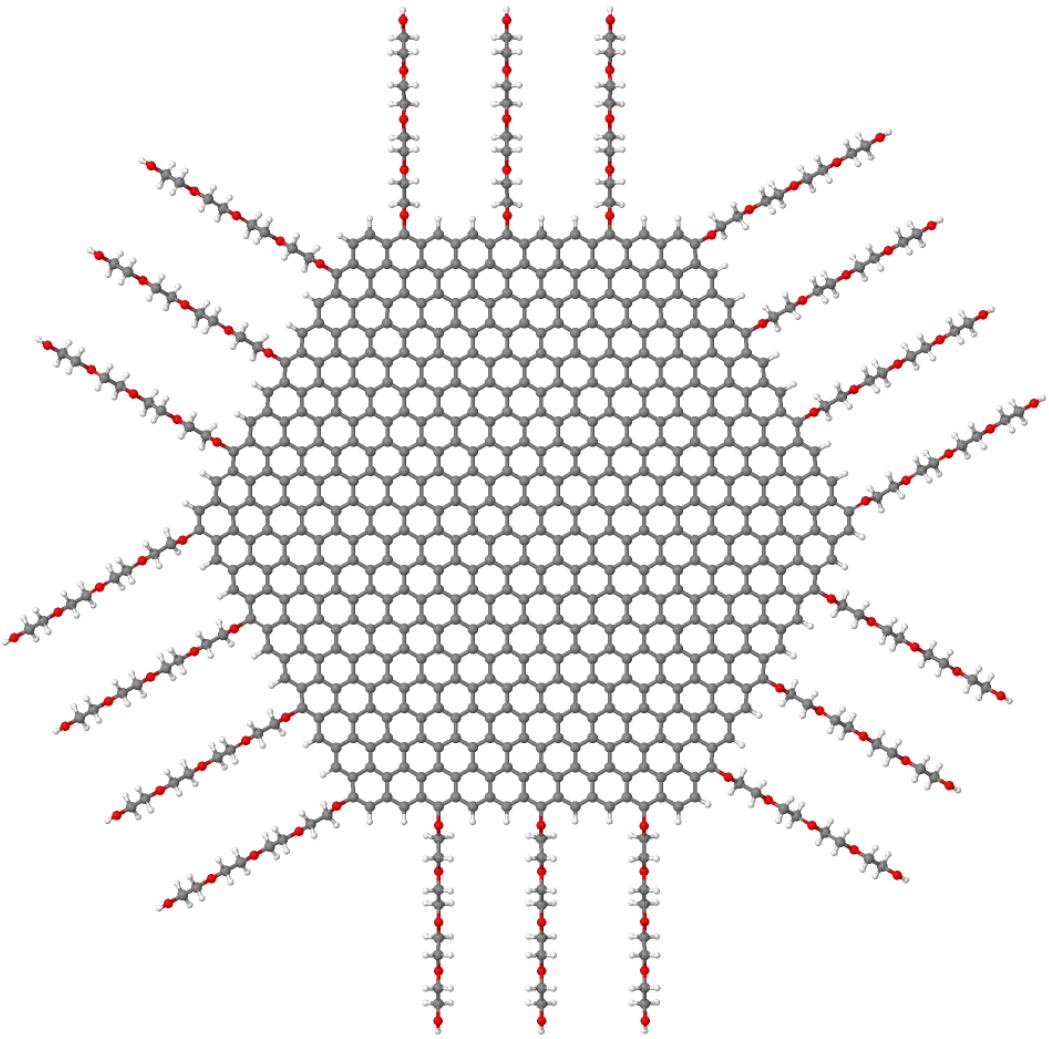

Figure 12: Representation of fPEG.

6.2. INPUT/OUTPUT

6.2.1. INPUT

During the work, we have used different types of programs to develop all the process. In this attachment we can see one of them.

```
Geometry = GenFormat {
264 C
H C O
   1     2           -0.0008307000           1.4255576100
0.0000000000
   2    2         1.2348648200        0.7130718800       -
0.0000000000
   3     2            1.2356985100         -0.7133132100
0.0000000000
[...]
 262    1        -0.3962450800       13.8453245100       -
0.0000000000
 263    1         7.0731888300       13.8278636200       -
0.0000000000
 264     1           11.7928837900           7.2653222000
0.0000000000
}
Driver = gDIIS {
  MovedAtoms = 1:-1
  MaxForceComponent = 1E-4
  MaxSteps = 1000
  OutputPrefix = "geom.out"
}
Hamiltonian = DFTB {
  SCC = Yes
  MaxSCCIterations = 1000
  SlaterKosterFiles = Type2FileNames {
    Prefix = "./mio-1-1/"
    Separator = "-"
    Suffix = ".skf"
  }
  MaxAngularMomentum {
    H = "s"
    C = "p"
    O = "p"
  }
  Filling = Fermi { Temperature [Kelvin] = 0.0 }
}
Driver = {}
Options = { WriteDetailedXML = Yes }
Analysis = { WriteEigenvectors = Yes }
ParserOptions = { ParserVersion = 4 }
```

6.2.2. OUTPUT

```
   Fermi distribution function

Geometry optimization step: 125

************************************************************
*************************
  iSCC Total electronic   Diff electronic      SCC error
    1   -0.11055933E+04   0.00000000E+00   0.81676432E-
05
************************************************************
*************************

 Coordinates of moved atoms (au):
    1      0.00006261      2.69291489     -0.00000000
[...]
  660     43.80544800      6.37713720      0.00000000


 Net atomic charges (e)
  Atom       Net charge
     1      -0.00014644
[...]
   660       0.07925975

 COMPONENT = q

 Eigenvalues /H
   -0.78219332
[...]
    1.04098955

 Fillings
     2.00000
[...]
     0.00000

 Nr. of electrons (up):   2460.00000000
 Atom populations (up)
  Atom       Population
     1       4.00014644
[...]
   660       0.92074025

 Fermi level:                          -0.1670569174 H
-4.5459 eV
 Band energy:                       -1088.1016015928 H
-29608.7511 eV
 TS:                                    0.0000000000 H
0.0000 eV
```

```
 Band free energy (E-TS):          -1088.1016015928 H
-29608.7511 eV
 Extrapolated E(0K):               -1088.1016015928 H
-29608.7511 eV
 Input/Output   electrons   (q):         2460.00000000
2460.00000000

 Energy H0:                        -1105.6257151265 H
-30085.6064 eV
 Energy SCC:                           0.0324095227 H
0.8819 eV
 Total Electronic energy:          -1105.5933056038 H
-30084.7245 eV
 Repulsive energy:                    43.4723067749 H
1182.9417 eV
 Total energy:                     -1062.1209988289 H
-28901.7829 eV
 Total Mermin free energy:         -1062.1209988289 H
-28901.7829 eV

 SCC converged

 Full geometry written in geom.out.{xyz|gen}

 Dipole moment   :    -0.00044609    -0.00038580    -
0.00000000 au
 Dipole moment   :    -0.00113384    -0.00098061    -
0.00000000 Debye

 Geometry converged
```